Chemical Engineering Journal 311 (2017) 163–172

Contents lists available at ScienceDirect

Chemical Engineering Journal

journal homepage: www.elsevier.com/locate/cej

Insights into the mechanism of persulfate activation with nZVI/BC nanocomposite for the degradation of nonylphenol

Imtyaz Hussain [a,b,c,*], Mingyu Li [a,b,*], Yongqing Zhang [c,d,e,*], Yichun Li [a,b], Shaobin Huang [c,d,e], Xiaodong Du [c], Guoqiang Liu [a,b], Waseem Hayat [c], Nazia Anwar [f]

[a] The Research Center of Water Treatment Technique and Material Engineering, Jinan University, Guangzhou, Guangdong Province, PR China
[b] School of Environment, Jinan University, Guangzhou 510632, PR China
[c] School of Environment and Energy, Guangdong Provincial Key Laboratory of Atmospheric Environment and Pollution Control, South China University of Technology, Guangzhou 510006, PR China
[d] State Key Laboratory of Pulp and Paper Engineering, South China University of Technology, Guangzhou 510640, PR China
[e] The Key Lab of Pollution Control and Ecosystem Restoration in Industry Clusters, Ministry of Education, Guangzhou 510006, PR China
[f] School of Computer Science and Engineering, South China University of Technology, Guangzhou 510006, PR China

HIGHLIGHTS

- nZVI/BC nanocomposite was successfully synthesized and characterized as PS activator.
- NP was effectively degraded at a wide pH range of 3.0–7.0 in nZVI/BC-PS system.
- The stability of nZVI/BC nanocomposite and effect of reaction parameters were investigated.
- $SO_4^{\cdot-}$ and ·OH radicals were identified in the system.

GRAPHICAL ABSTRACT

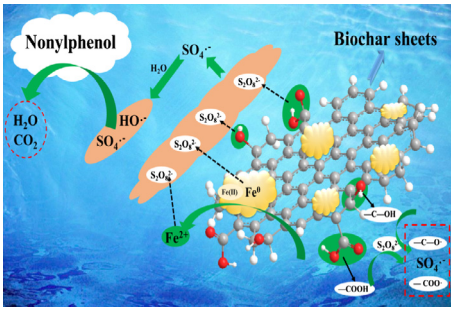

ARTICLE INFO

Article history:
Received 11 August 2016
Received in revised form 10 November 2016
Accepted 11 November 2016
Available online 12 November 2016

Keywords:
nZVI/BC
Persulfate
NP
Degradation
EPR

ABSTRACT

Nonylphenol (NP) is an endocrine disrupting chemical which is capable of interfering with the hormonal system of various organisms in the environment. In this study, nanoscale zero-valent iron (nZVI) supported on biochar (BC) nanocomposite (nZVI/BC) was synthesized using low-cost rice husk through reduction of ferrous iron with sodium borohydride as a reductant under nitrogen atmosphere. The morphology and structure of nanocomposite was characterized by X-ray diffraction, scanning electron microscopy, Fourier transform infrared spectroscopy and Brunauer-Emmett-Teller studies. The synthesis nZVI/BC nanocomposite is used as an efficient persulfate (PS) activator to generate sulfate radicals ($SO_4^{\cdot-}$) for the degradation of NP. The degradation efficiency of NP (20 mg/L) was 96.2% within 120 min using initial dosage of 0.4g/L nZVI/BC_3 and concentrations of 5 mM persulfate. The effects of reaction parameters such as initial pH, PS concentration and dosage of nZVI/BC_3 nanocomposite were investigated. The presence of oxygen functional groups on the surface of BC and large surface area, nZVI/BC nanocomposite increased generation of $SO_4^{\cdot-}$ which enhanced NP degradation. The radical scavenger experiments and electron paramagnetic resonance (EPR) studies showed that both $SO_4^{\cdot-}$ and ·OH were responsible for degradation of NP. The findings of this study provide new insights into the mechanism of nZVI/BC activating persulfate and its potential applications for the treatment of wastewater.

* Corresponding authors at: The Research Center of Water Treatment Technique and Material Engineering, Jinan University, Guangzhou, Guangdong Province, PR China (I. Hussain and M. Li). School of Environment and Energy, Guangdong Provincial Key Laboratory of Atmospheric Environment and Pollution Control, South China University of Technology, Guangzhou 510006, PR China (Y. Zhang).
E-mail addresses: imtiazuaf@yahoo.com (I. Hussain), limingyu2000@163.com (M. Li), zhangyq@scut.edu.cn (Y. Zhang).

http://dx.doi.org/10.1016/j.cej.2016.11.085
1385-8947/

1. Introduction

Endocrine disrupting chemicals (EDCs) existence in the environment has become a topic of main concern all over the world. Nonylphenol (NP) is one of the most abundant EDCs present in the environment capable of interfering with the hormonal system of various organisms [1,2]. NP is used as raw material in the manufacture of nonylphenol ethoxylates (NPEOs) which are nonionic surfactants widely used in industrial, agricultural, and household products. Over 60% of the total NPEOs manufactured go into the aquatic environment due to extensive use of NPEOs and NPEOs produce NP in the environment [3]. The bioaccumulation of NP at low concentrations in the aquatic environment can be a source of disruption of the endocrine system of aquatic organisms. NP mimics the natural 17b-estradiol hormone by competing for the binding site of the receptor's natural estrogen due to their structural similarity. The toxicity of NP causes oxidative stress and apoptosis in various organisms [3,4]. NP annual production reached 73,500 tons in Europe, 154,200 tons in USA, 16,000 tons in China, 16,500 tons in Japan [1,3,5]. The European Union has restricted production and use of NP since 2003 and NP concentration limited to 2 μg/L in water bodies [6]. The main pathway of exposure to NP for human and wildlife is via water. Hence, it is important to develop novel and consistent treatment approaches to remove NP from wastewaters.

Currently, advanced oxidation processes (AOPs), which are based on the production of reactive radical species, are considered as one of the most powerful and attractive methods for the degradation of recalcitrant organic pollutants [7]. In recent years, sulfate radical based AOPs have been recognized as promising technologies for the degradation and mineralization of refractory contaminants [8–11]. $SO_4^{\cdot-}$ has higher redox potential (E_0 = 2.5–3.1 V) as compared to hydroxyl radical (·OH) (E0 = 1.8–2.7 V), which makes the $SO_4^{\cdot-}$ more efficient for the removal of contaminants [12,13]. $SO_4^{\cdot-}$ has strong oxidizing ability, longer half-life and higher reactivity over wide pH range [13–14]. Generally, $SO_4^{\cdot-}$ can be generated by the activation of persulfate (PS) through heat [15,16], UV [17], transition metals [18,19], ultrasound [20] and base [21]. PS has been proven to be the most effective oxidant in AOPs for the removal of organic compounds from groundwater, soil and wastewater [22,23].

Zero valent iron (ZVI) is cheap, non-toxic and act as potential alternative source of Fe^{2+} through the dissociation of ZVI under both aerobic and anaerobic conditions. ZVI has been successfully used to activate PS producing $SO_4^{\cdot-}$ for the removal of 4-chlorophenol [24], polyvinyl alcohol, 2, 4-dinitrotoluene [8,25], p-chloroaniline, aniline [9,26] and alachlor [27]. nZVI can produce Fe^{2+} by the following reactions.

$$Fe^0 \rightarrow Fe^{2+} + 2e^- \quad (1)$$

$$Fe^0 + S_2O_8^{2-} \rightarrow Fe^{2+} + 2SO_4^{2-} \quad (2)$$

$$Fe^0 + H_2O + 0.5O_2 \rightarrow Fe^{2+} + 2OH^- \quad (3)$$

$$Fe^0 + 2H_2O \rightarrow Fe^{2+} + H_2 + 2OH^- \quad (4)$$

$$S_2O_8^{2-} + Fe^{2+} \rightarrow Fe^{3+} + SO_4^{2-} + SO_4^{\cdot-} \quad (5)$$

The activation of PS enhanced by nanoscale zero valent iron (nZVI) due to its large surface area, small particle size and high reactivity [10]. Though, the surface area, reactivity and mobility of nZVI particles decrease by agglomeration of nZVI into microscale particles due to high surface energies and intrinsic magnetic interactions of nZVI particles. The reactivity of nZVI also decreases by oxidation when nZVI contact with air [28]. In order to overcome the problem, different types of supporting materials such as rectorite, resin, active carbon, zeolite, and graphene have been used for the better dispersion of nZVI [29–33]. Nonetheless, a good supporting material should be efficient, safe, inexpensive, and has ability to prevent the agglomeration of bare-nZVI.

Biochar (BC) is a pyrogenic carbon rich material which is generated by pyrolysis of biomass under limited oxygen conditions. The application of BC has gained more attention for the remediation of pollutants from soil and water and makes it an effective and indispensable environmental remediation material [34,35]. BC has high surface area, porous structure and abundant oxygen-containing functional groups such as hydroxyl (–OH) and carboxyl (–COOH) on its surface. Therefore, BC has been used as effective and low-cost adsorbents for the removal of organic pollutants and heavy metals. Because of its multi-functional features, BC has been employed as mechanical supporting material for the dispersion and stabilization of engineered nanoparticles to improve their environmental application [36,37].

In this work, a biochar supported nZVI composite (nZVI/BC) was synthesized and observed as an effective activator of persulfate to generate $SO_4^{\cdot-}$ for the degradation of NP from aqueous solution. The obtained nZVI/BC composite was demonstrated to be highly effective for improved catalytic oxidation of NP with PS as an oxidant. The objectives of present study are to 1) synthesize and characterize a novel nZVI/BC composite; 2) assess the activation of PS efficiency with nZVI/BC composite to facilitate NP degradation in aqueous solution; 3) recognize the dominant radical generating from PS decomposition and resulting in NP removal; 4) explore the PS activation mechanism by nZVI/BC.

2. Experimental

2.1. Materials and chemicals

Nonylphenol ($C_{15}H_{24}O$, CAS Nr. 84852-15-3, molecular weight 220.35 g/L) sodium borohydride (NaBH4) (>98%), 5,5-dimethyl-1-pyrroline-N-oxide (DMPO) were obtained from Aladdin Reagents Co. Ltd. (Shanghai, China). All other chemicals used in this study were analytical reagent grade and deionized water was used throughout this study.

2.2. Synthesis of nZVI/BC

The biochar was produced by the pyrolysis of rice husk as the raw biomass material. The rice husk was collected from Guangzhou, Guangdong province, China. The collected material was washed several times with deionized water to remove impurities and then oven dried at 80 °C. The dried rice husk was placed in ceramic crucibles covered with fitting lids and then pyrolyzed in a muffle furnace for 2 h at a temperature of 400 °C under oxygen-limited condition. The obtained BC was treated by rinsing with 1 M HCl to remove inorganic components followed by soaking with distilled water to remove any residual acids. In this study, nZVI was synthesized by reduction method using $NaBH_4$ as reducing agent which reduce Fe^{2+} to nZVI (Eq. (6))

$$2Fe^{2+} + BH_4^- + 2H_2O \rightarrow 2Fe^0 + BO_2^- + 2H_2 + 4H^+ \quad (6)$$

The nZVI/BC was synthesized according to reported method [38] by reducing ferrous iron ($FeSO_4{\cdot}7H_2O$) with sodium borohydride ($NaBH_4$) as a reductant. In a classic procedure, 0.756 g of BC was dissolved in freshly prepared 250 ml solution of $FeSO_4{\cdot}7H_2O$ (0.054 M) and the mixture was stirred dynamically at ambient temperature for 1 h to attain homogenous solution. The solution was degassed by purging N_2 for 1 h and the whole preparation process was under N_2 atmosphere. Then equal volume of $NaBH_4$

(0.108 M) solution was added dropwise for the reduction of $FeSO_4 \cdot 7H_2O$ to nZVI with vigorous stirring at room temperature. After the completion of reaction, the black nZVI/BC particles were separated from the solution by vacuum filtration (0.45 μm membrane filter). Afterward, nZVI/BC nanocomposite was washed several times with ethanol and deionized water and then vacuum dried at 60 °C. The synthesized nZVI/BC nanocomposite was labeled as 1:1 mass ratio of nZVI to BC. Four types of nZVI/BC nanocomposites were synthesized with different mass ratios of nZVI to BC at 1:1, 1:2, 1:3 and 1:4, respectively. The nanocomposites were labeled $nZVI/BC_1$, $nZVI/BC_2$, $nZVI/BC_3$ and $nZVI/BC_4$, respectively

2.3. Characterizations

The surface morphology of BC, nZVI and nZVI/BC nanocomposite was observed with EVO 18 (Car Zeiss) scanning electron microscope (SEM) being operated at an acceleration voltage of 10 kV. The crystal structures BC, nZVI and nZVI/BC were characterized by X-ray diffractometer (XRD, D8 Advance, Bruker) with Cu Kα radiation ($\lambda = 1.5408$ nm) over a 2θ range of 10°–80°. The infrared spectra were recorded on a Fourier transform infrared (FTIR) spectrophotometer. The spectra were obtained from 400 to 4000 wave numbers (cm^{-1}) using a Vector 33 (Bruker, German). Autosorb-iQ2PM (Quanta chrome instrument US) an automate vapor sorption and surface area analyzer instrument was used to measure Brunauer-Emmett-Teller (BET) specific surface area and pore volume of BC, nZVI and nZVI/BC.

2.4. Experimental process

A stock solution of NP was prepared at 1000 mg/L in methanol and stored in the dark at 4 °C. PS stock solution (50 mM) was prepared in a 100 mL volumetric flask with deionized water. All experiments were performed in 250 ml Erlenmeyer flasks under constant stirring in a rotary shaker at 25 °C and 125 rpm. For NP degradation experiments, predetermined amount of BC (0.4g/L), nZVI (0.4g/L) and nZVI/BC with different mass ratios of 1:1, 1:2, 1:3 and 1:4 were added into 100 ml of 20 mg/L NP solution and followed by adding 5 mM PS solution at pH 7.0. The initial pH of NP solution was adjusted by 0.1 M H_2SO_4 and 0.1 M NaOH. At regular time intervals, 5 ml sample was taken and filtered through 0.22 μm syringe filters prior to analysis. After filtration, samples were quenched immediately with sodium thiosulfate to stop the reaction. Various parameter effects on the degradation of NP, including dosage of nZVI/BC, solution pH, PS concentration of the NP solution were investigated. All these experiments were performed in triplicate.

2.5. Analytical methods

The concentrations of NP samples were determined by UV spectrophotometer. The degradation efficiency of NP was calculated by using the following equation:

$$\text{Degradation efficiency}(\%) = (C_0 - C_e)/C_0 \times 100 \quad (7)$$

where, C_0 was the initial concentration of NP and Ce was the concentration at time t. Fe^{2+} concentration was measured by colorimetrically with 1,10-phenanthroline using spectrophotometer at 510 nm [39]. Persulfate anion concentration was determined by spectrophotometric method with potassium iodide [40]. The mineralization of NP was determined by EMENTAR LiquiTOC Total Organic Carbon (TOC) analyzer. An electron paramagnetic resonance spectrometer (EPR) (Bruker, A300 microx) was used to determine the production of sulfate and hydroxyl radicals. DMPO (0.1 M) was used as the radical spin-trapping reagent. The EPR determination was performed under the following conditions: a center field of 3517 G, a microwave power of 20.16 mW, a microwave frequency of 9.875 GHz, a sweep width of 250 G, a modulation frequency of 100 kHz, a receiver gain of 3.99×10^4, modulation amplitude of 1.00 G, a sweep time of 122.8 s.

3. Results and discussion

3.1. Characterization of nZVI/BC composite

The physicochemical properties of BC, nZVI and nZVI/BC are displayed in Table 1. It can be depicted in Table 1 that the surface area of nZVI and BC was 52.16 m^2/g and 194.35 m^2/g, respectively. The surface area of $nZVI/BC_1$, $nZVI/BC_2$, $nZVI/BC_3$ and $nZVI/BC_4$ was 96.13, 107.51, 122.65, 119.11 m^2/g, respectively. The observation showed that surface area of nZVI/BC nanocomposite increased with increasing BC contents because higher BC contents in nZVI/BC composite were promising for nZVI dispersion on the surface of BC. However, the surface area of $nZVI/BC_4$ was decreased by further increase of BC contents due to increasing aggregation of BC sheets.

The representative SEM images of BC, nZVI and $nZVI/BC_3$ were shown in Fig. 1. BC morphology was characterized by rough and porous shape (Fig. 1a). As can be seen in Fig. 1b, the shape of synthesized nZVI particles was spherical with particle sizes range of nanoscale. The morphology of nZVI also showed that nZVI existed as chain-like aggregates due to magnetic interaction between small particles. It can be found from the SEM image in Fig. 1c, the surface of $nZVI/BC_3$ was entirely different from that of the BC due to distribution of nZVI particles on the surface of BC. The results demonstrated that the occurrence of both iron and BC in the composite confirmed through SEM images and nZVI particle homogenously dispersed on BC surface. Hence, $nZVI/BC_3$ composite morphology observed by SEM obviously shows that nZVI are able to distribute on BC with nanoscale. The results also showed that BC has well prospective ability to prevent the aggregation of nZVI and act as good carrier of nZVI.

The crystalline structures of nZVI, BC and nZVI/BC were investigated by XRD analysis. The XRD patterns of nZVI, BC and nZVI/BC are shown in Fig. 2a. The XRD representative peak at 2θ = 45° confirmed the presence of α-Fe^0. The apparent peak at 2θ = 20–25° in XRD patterns was allotted to the graphite structure of BC [12,38] In the XRD diffractogram of nZVI/BC, both representative diffraction peaks of BC and nZVI showed successful synthesis of nZVI/BC composites. The surface functional groups of BC and nZVI/BC were observed by FTIR spectroscopy. Fig. 2b showed the FTIR spectra of BC and nZVI/BC. The spectrum of BC and nZVI/BC revealed a broad band at about 3400 cm^{-1}, which is associated to –OH groups, showing the presence of hydroxyl groups on the surface of material. The band spectrum at 1600 $cm^{-1}$was assigned to the stretching vibration of carbonyl/carboxyl C=O. The peak at 1101 cm^{-1} can be assigned to the stretching vibration of C–O from phenolic group [41,42]. The peak at 665 cm^{-1} in the spectrum of the nZVI/BC might be ascribed to the stretching vibration of Fe–O–H [38].

Table 1
Physiochemical properties of the nZVI, BC and nZVI/BC nanocomposite.

Catalyst	BET surface area (m^2/g)	Pore volume (cm^3/g)	Pore width (nm)
nZVI	52.16	0.005	8.11
BC	194.35	0.098	2.12
$nZVI/BC_1$	96.13	0.017	1.74
$nZVI/BC_2$	107.51	0.024	1.86
$nZVI/BC_3$	122.65	0.031	1.97
$nZVI/BC_4$	119.11	0.041	2.15

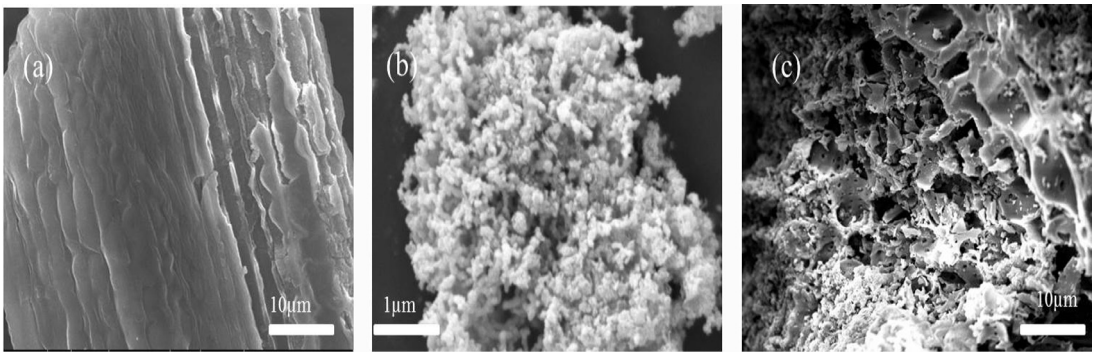

Fig. 1. SEM images of BC (a), nZVI (b), nZVI/BC_3 (c).

3.2. Degradation of NP by nZVI/BC-PS system

The experiments were conducted to examine the degradation efficiency of NP by BC, nZVI, and with different ratios of nZVI/BC (1:1–1:4) composite without PS. Fig. 3a shows that the adsorption of NP was 10.9% and 16.87% by BC and nZVI respectively. As shown in Fig. 3a, the removal efficiency of NP increased from 23.5% to 38.52% with an increase in nZVI/BC ratio from 1:1 to 1:3. This might be due to the fact that biochar increases the dispersivity of nZVI particles through adhesion of nZVI on the rough and porous surface of BC. The removal efficiency of NP increased due to availability of more adsorption sites [43,44]. However further increase in the nZVI: BC ratio from 1:3 to 1:4, NP removal efficiency was decreased to 33.3%. At higher nZVI/BC ratio, nZVI particles may enclose by the excess amount of BC compared to the optimum dosage, therefore obstructing the direct contact of nZVI with NP in the aqueous solution which resulted in the decreased removal efficiency of NP.

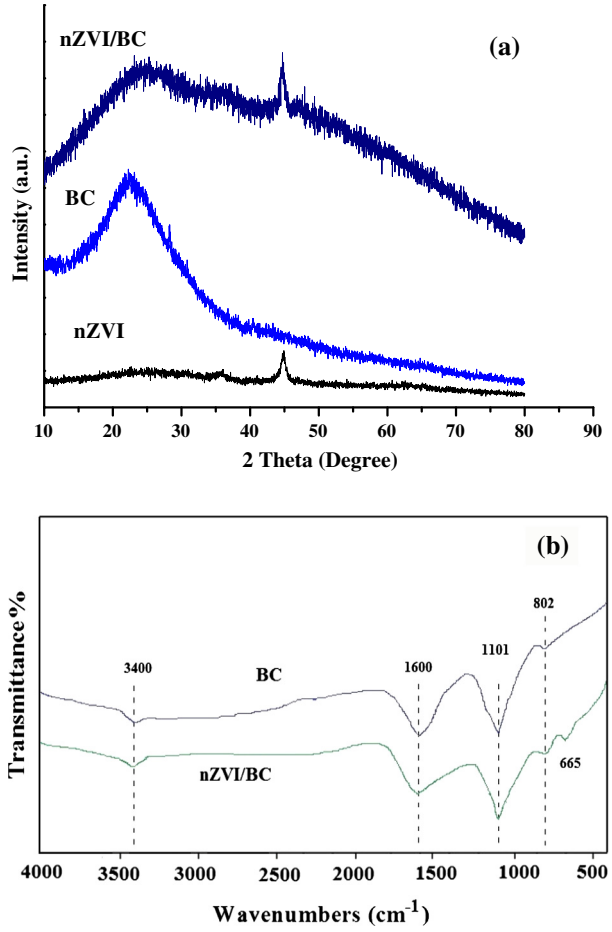

Fig. 2. XRD patterns (a) and FT-IR spectra (b) of nZVI, BC and nZVI/BC_3.

Fig. 3b showed the degradation of NP with nZVI, BC and nZVI/BC composite with different mass ratios (1:1–1:4) in the presence of PS. When PS alone was added to the NP solution, 7.1% NP was degraded due to limited oxidation ability of PS (E^0 = 2.01 V) [8]. As depicted in Fig. 3c, PS consumptions percentage was 6.2% after 120 min reaction in PS alone system, showing that small amount of PS was decomposed in this condition. In the BC/PS system, 28.3% NP degradation efficacy was observed and PS consumptions percentage was 15.3%, showing that BC has weak activation capability of persulfate. While in the nZVI/PS system, NP degradation efficiency was increased to 61.72% compared to 28.3% for BC/PS system and decomposition of PS was 47.1%. However, the degradation efficiencies of NP were 68.4%, 78.31%, 96.2%, and 88.63% for the nZVI/BC mass ratios of 1:1, 1:2, 1:3 and 1:4, respectively. In addition, PS consumption was increased from 47.1% to 85%. The results showed that nZVI and nZVI/BC catalyst could effectively activate PS to generate sulfate radical through Eq. (5) and then hydroxyl radical would be generated by the reaction between sulfate radical and water (Eq. (8). nZVI/BC nanocomposite has higher surface area as compared to nZVI which enhanced the activation site for persulfate. It can be seen that NP degradation efficiency increased and reached at 96.2% at optimum ratio of nZVI/BC_3. The dispersion of nZVI particles on the surface of BC between the layers helped to avoid the aggregation of BC sheets [45,46]. The results showed that more amount of BC in nZVI/BC nanocomposite seemed to be more promising for the degradation of NP. Nevertheless, excess amount of BC in nZVI/BC_4 nanocomposite did not show more synergistic effect for the degradation of NP. Therefore, NP degradation efficiency was decreased to 88.63% with nZVI/BC_4. The reason is that excessive BC may block the reactive sites of iron surface and causes the aggregation of BC sheets [45,46] Therefore, the nZVI/BC_3 was found to be optimum and was selected for further study.

$$SO_4^{\cdot-} + H_2O \rightarrow SO_4^{2-} + {\cdot}OH + H^+ \quad (8)$$

3.3. Effect of nZVI/BC_3 and PS dosage on NP degradation

The degradation efficiency of NP was evaluated at different nZVI/BC_3 dosage from 0.1 to 0.5 g/L whereas keeping concentrations of NP at 20 mg/L and PS at 5 mM. As observed, the removal efficiency of NP was significantly influenced by the dosage of nZVI/BC_3. As can be shown in Fig. 4a, NP degradation increased rapidly from 54.5% to 96.2% after 120 min with increasing dosage of nZVI/BC_3 from 0.1 to 0.4 g/L. NP degradation increased when nZVI/BC_3 dosage was increased due to more generation of sulfate

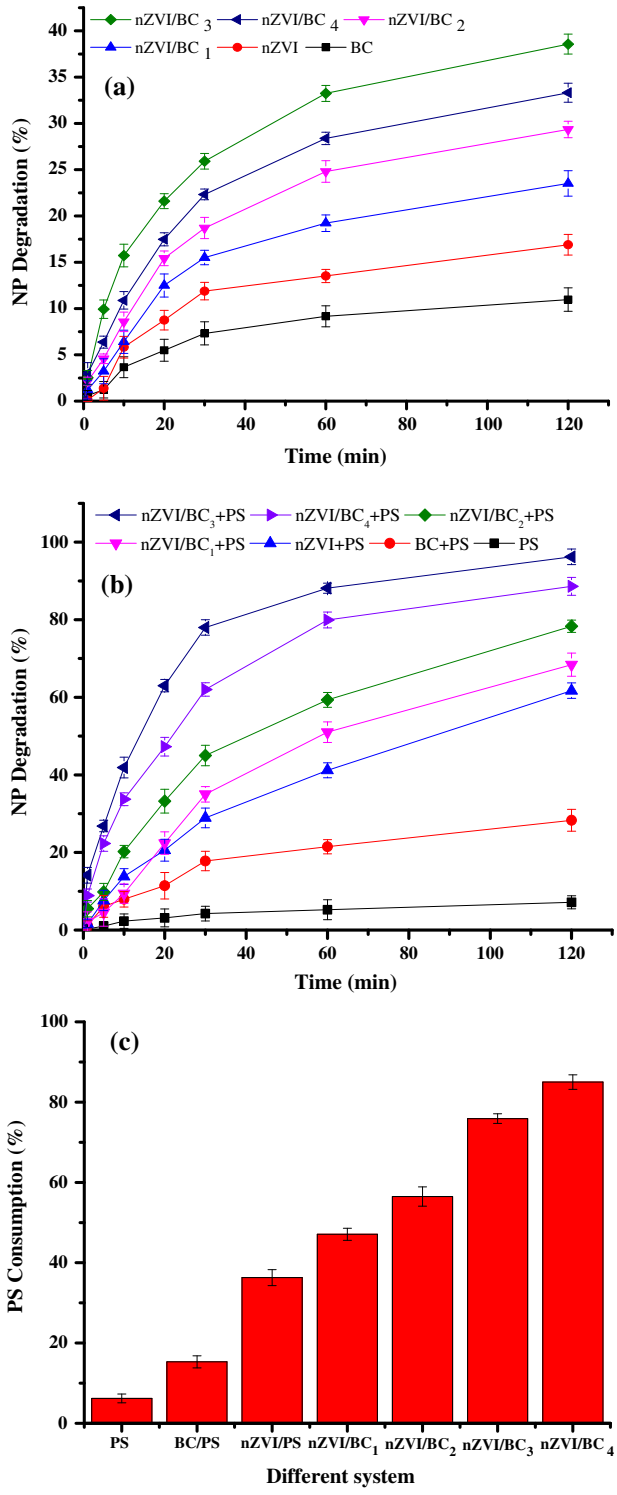

Fig. 3. Degradation of NP in different system; (**a**) without PS and (**b**) with PS. [NP] = 20 mg/L; [BC] = 0.4 g/L; [nZVI] = 0.4 g/L; nZVI/BC_1 (mass ratio of 1:1), nZVI/BC_2 (mass ratio of 1:2), nZVI/BC_3 (mass ratio of 1:3) nZVI/BC_4 (mass ratio of 1:4), [PS] = 5.0 mM; Temp = 25 °C; pH = 7.0 (**c**) consumption of PS.

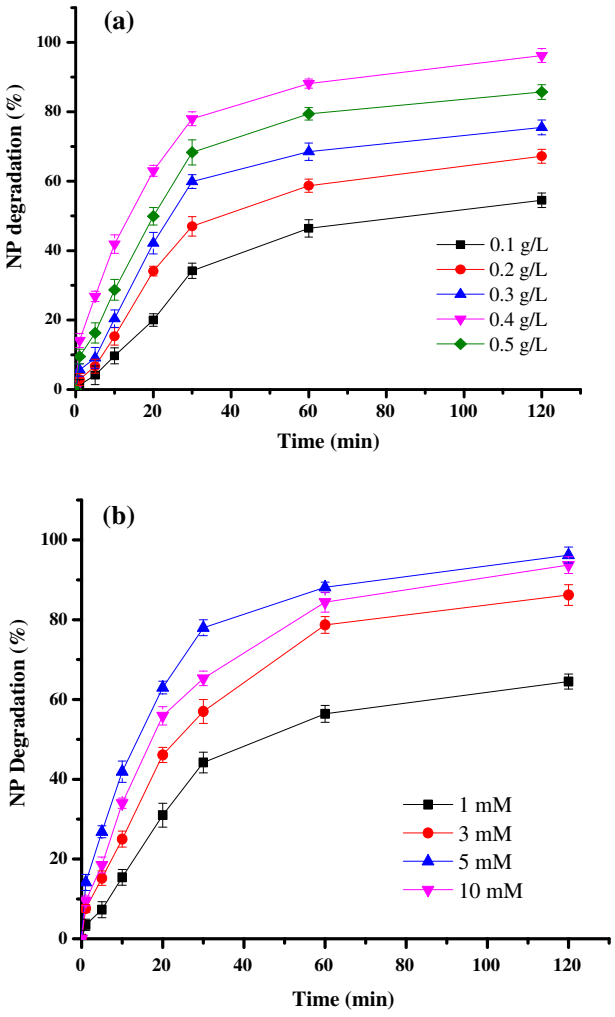

Fig. 4. (**a**) Effect of nZVI/BC_3 dosages on the degradation of NP; (**b**) Effect of PS concentrations on the degradation of NP. [NP] = 20 mg/L; [PS] = 5.0 mM; Temp = 25 °C; pH = 7.0.

radical. The results revealed that more Fe^{2+} would be released with the higher addition of nZVI/BC_3, finally facilitating the decomposition of PS to generate $SO_4^{\cdot-}$. Overall, the increase of nZVI/BC_3 dosage could result in more generation of $SO_4^{\cdot-}$ due to availability of more active sites for PS decomposition [47], finally enhancing the degradation of NP. However, the degradation of NP was decreased to 85.7% when nZVI/BC_3 dosage was increased to 0.5 g/L, PS consumption increased and large concentration of $SO_4^{\cdot-}$ are produced, leading to scavenging reaction without degradation of NP. In addition, excess Fe^{2+} could scavenge $SO_4^{\cdot-}$ produced in nZVI/BC-PS system (Eq. (9)) [12,9,26].

$$SO_4^{\cdot-} + Fe^{2+} \rightarrow Fe^{3+} + SO_4^{2-} \quad (9)$$

The effect of PS concentrations on NP degradation was explored with a fixed dosage of nZVI/BC_3 (0.4 g/ and pH 7.0) in nZVI/BC_3-PS system. Four different PS concentrations of 1, 3, 5, 10 mM were used in this study to determine the optimum PS concentration. As seen in Fig. 4b, the degradation efficiency NP increased from 42.5% to 96.2% with the increasing of PS concentration from 1 mM to 5 mM. However, the degradation efficiency of NP decreased with the further increase in PS concentration up to 10 mM. With the increasing concentration of PS, large amounts of $SO_4^{\cdot-}$ were produced due to the higher concentration of PS, which resulted in enhanced NP degradation. Nevertheless, high concentration of $SO_4^{\cdot-}$ could also be scavenged by itself and react with $S_2O_8^{2-}$ to form $S_2O_8^{\cdot-}$ and SO_4^{2-} as shown in Eqs. (10) and (11), causing the decreasing degradation of NP.

$$SO_4^{\cdot-} + S_2O_8^{2-} \rightarrow SO_4^{2-} + S_2O_8^{\cdot-} \quad (10)$$

$$SO_4^{\cdot-} + SO_4^{\cdot-} \rightarrow S_2O_8^{2-} \quad (11)$$

3.4. Effect of initial pH on NP degradation

The pH of the solution plays a significant role in determining the degradation of NP and greatly affects the presence of reactive species in the solution. The experiments were conducted at different pH 3.0, 5.0, 7.0, 9.0 and 11.0 to investigate the effect of initial pH on NP degradation. It can be clearly seen in Fig. 5a that NP degradation efficiency is higher at acidic pH than at alkaline pH. The order of NP degradation efficiencies was pH 3.0 > pH 5.0 > pH 7.0 > pH 9.0 > pH 11.0. The results showed that pH significantly influenced the degradation efficiency of NP. It was observed that the degradation of NP increased from 55.9% to 99.15% as the solution pH decreased from 11.0 to 3.0 and NP degradation efficiency was reached the maximum at pH 3.0. The results were in agreement with our previous work that acidic pH (pH 3.0) favored the degradation of *p*-chloroaniline and aniline in ZVI-PS system [9,26]. However, acidic condition could result in the rapid corrosion of nZVI and release more Fe^{2+} [48]. Under acidic conditions, extra sulfate radical could be produced due to further acid catalyzation according to the following equations. The degradation of NP increased due to production of high radical concentrations and almost complete degradation of NP was achieved.

$$S_2O_8^{2-} + H^+ \rightarrow HS_2O_8^- \quad (12)$$

$$HS_2O_8^- \rightarrow SO_4^{\cdot-} + SO_4^{2-} + H^+ \quad (13)$$

Under basic conditions, more hydroxyl radical produced through sulfate radical reaction with H_2O or OH^- (Eqs. (8) and (14))

$$SO_4^{\cdot-} + OH^- \rightarrow SO_4^{2-} + {}^{\cdot}OH \quad (14)$$

Fig. 5a also showed that the degradation of NP decreased as initial pH of solution increased, the removal of NP was still 70.15% and 55% at pH 9.0 and 11.0, respectively. Consequently, under alkaline conditions NP degradation efficiency was lower when compared to acidic and neutral conditions. As shown in Fig. 5b, the solution pH declined due to the formation of bisulfate (HSO_4^-) byproduct by decomposition of persulfate. The promising degradation results revealed that nZVI/BC_3-PS system could be used over a wide range of pH values (pH 3.0–11.0).

3.5. Effect of temperature on NP degradation

The effect of the reaction temperature on the activation of persulfate over nZVI/BC_3 was investigated at 15, 25, 35 and 45 °C. The results revealed that the reaction temperature has a significant effect on NP degradation (Fig. 6). The degradation efficiency of NP remarkably increased with increasing temperature. As shown in Fig. 6, the performance of nZVI/BC_3 for PS activation was increased at elevated temperature. For instance 72% and 96.2% of NP was removed after 120 min at 15 and 25 °C, respectively. Whereas, a complete NP degradation was achieved in 120 and 30 min at 35 and 45 respectively. This might be attributed to the enhanced generation of sulfate radicals by PS activation at high temperatures and results in faster degradation of NP in aqueous solution. The results also confirmed that NP degradation followed the pseudo-first-order kinetic model. NP degradation rate constants at 15, 25, 35 and 45 °C were calculated to be 0.0245, 0.0483, 0.0856 and 0.181 min^{-1}, respectively. Furthermore, the activation energy for the degradation of NP was calculated based on the pseudo-first-order rate constants by using Arrhenius equation, $\mathrm{Ln}k = \mathrm{Ln}\ A - Ea/RT$, where R is the universal gas constant (8.314 J mol^{-1} K^{-1}), A is the pre-exponential factor, Ea is the apparent activation energy, and T is the absolute temperature. A good linear correlation between ln k and 1/T (R^2 = 0.997) was observed. The value of activation energy of the reaction was calculated to be 43.45 kJ mol^{-1}.

Moreover, the other parameters of activation such as entropy (ΔS) and enthalpy (ΔH) were calculated by employing Eyring

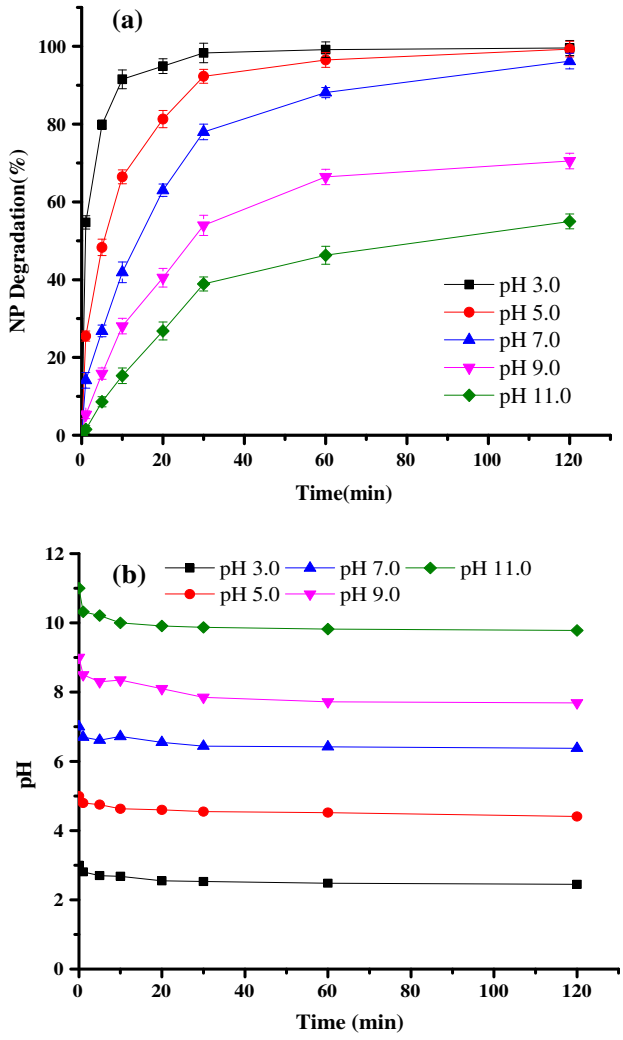

Fig. 5. (**a**) Effect of of initial pH on the degradation of NP; (**b**) The variation of pH values [NP] = 20 mg/L; [PS] = 5.0 mM; Temp. = 25 °C; [nZVI/BC_3] = 0.4 g/L.

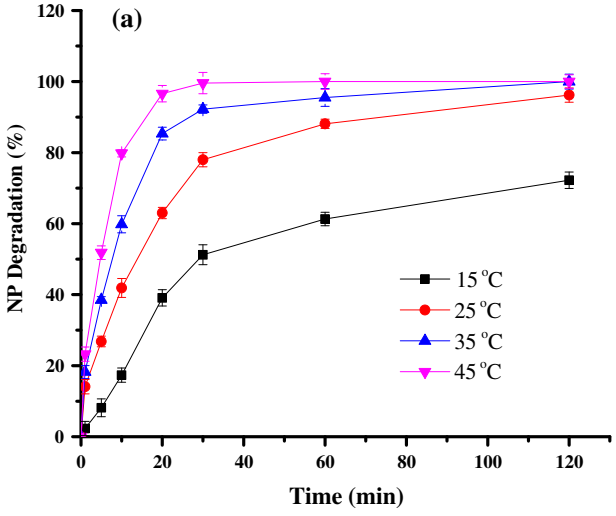

Fig. 6. (**a**) Effect of temperature on the degradation of NP; (**b**) The plot of ln(*k*/*T*) versus *1*/*T* [NP] = 20 mg/L; [PS] = 5 mM; [nZVI/BC_3] = 0.4 g/L pH = 7.0.

equation and rate constants. The general form of the Eyring equation as given in the following equation.

$$k = \frac{k_B T}{h} e^{-\frac{\Delta G}{RT}} \quad (15)$$

where G is the Gibbs free energy of activation, which is given as:

$$\Delta G = \Delta H - T \cdot \Delta S \quad (16)$$

The Eyring equation is obtained by substituting equation (16) into Eq. (15)

$$\ln \frac{k}{T} = -\frac{\Delta H}{R} \cdot \frac{1}{T} + \ln \frac{kb}{h} + \frac{\Delta S}{R} \quad (17)$$

where R is gas constant (8.314 J mol^{-1} K^{-1}), h is Planck's constant (6.626×10^{-34} J s), k is rate constant, k_B is Boltzmann constant (1.38×10^{-23} J K^{-1}) and T is absolute temperature.

According to Eq. (17), the Eyring plot of ln(k/T) versus $1/T$ provides a straight line with intercept of ln(k_B/h) + $\Delta S/R$ and slope of $-\Delta H/R$ from which ΔS and ΔH was calculated to be −115.23 J mol^{-1} K^{-1} and 41.19 kJ mol^{-1}, respectively. According to Eq. (16), Gibbs free energy (ΔG) was calculated to be 75.53 kJ mol^{-1}.

3.6. Identification of predominate radical species in the nZVI/BC-persulfate system

It has been observed that ·OH would produce through reaction of $SO_4^{\cdot-}$ with hydroxyl ion under alkaline conditions (Eq. (14)). In addition, ·OH can also produce by the reaction between $SO_4^{\cdot-}$ and H_2O at all pHs (Eq. (8)) [49]. It is well recognized that the chemical probe process has successfully used to identify activity of $SO_4^{\cdot-}$ and ·OH towards contaminants in oxidation processes [50]. So, the quenching experiments were performed to identify the dominant reactive species in nZVI/BC_3-persulfate system at different pH values. Two kinds of alcohols, ethanol (EtOH, containing α-hydrogen) and tert-butyl alcohol (TBA, without α -hydrogen) were used to examine the roles of $SO_4^{\cdot-}$ and ·OH for the degradation of NP. EtOH is an effective scavenger for both $SO_4^{\cdot-}$ and ·OH and the reaction rate constants of EtOH with $SO_4^{\cdot-}$ and ·OH are 1.6–7.7 × 10^7 M^{-1} s^{-1} and 1.2–2.8 × 10^9 M^{-1} s^{-1} respectively. TBA acts as strong quenching agent for ·OH and has 418–1900 times higher rate constant with ·OH (3.8–7.6 × 10^8 M^{-1} s^{-1}) than with $SO_4^{\cdot-}$ (4–9.1 × 10^5 M^{-1} s^{-1}) [38,51]. Therefore, EtOH and TBA were added into the reaction solution as quenching agents to elucidate dominant reactive species.

Table 2 showed the results obtained for NP degradation with and without scavenging agents. It seemed that both EtOH and TBA exerted significant inhibiting effect on the degradation efficiency of NP at pH 3.0. With the addition of 0.1 M EtOH and 0.1 M TBA into reaction solution, the degradation process was significantly inhibited with removal efficiency decreasing from 99.15% to 7.2% and 99.15% to 47.13%, respectively. The results revealed that radical quenching effect for EtOH was higher than that for TBA. It indicated that $SO_4^{\cdot-}$ was the predominant radical

Table 2
Effect of ethanol and TBA on the degradation of NP (20 mg/L) in the presence of nZVI/BC_3 (0.4 g/L) and PS (5.0 mM) under different initial pH values at 25 °C.

	NP degradation (%)			Main radicals
pH	Blank[a]	Ethanol	TBA	
3	99.15	7.2	47.13	$SO_4^{\cdot-}$
7	96.2	15.54	39.61	$SO_4^{\cdot-}$/·OH
11	55	18.6	28.2	$SO_4^{\cdot-}$/·OH

[a] "Blank" means no alcohols addition.

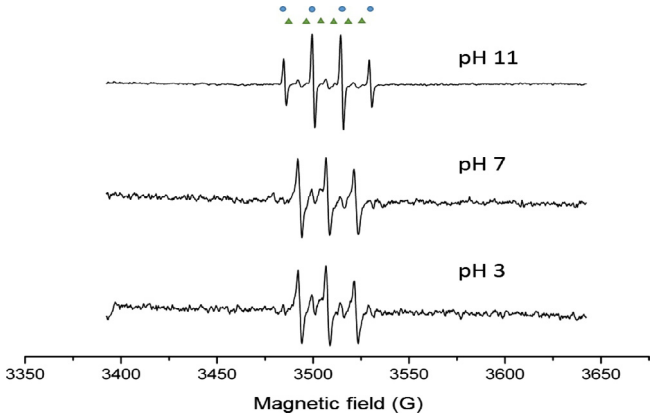

Fig. 7. EPR spectra of $SO_4^{\cdot-}$ and ·OH free radical adducts at different pH (3.0. 7.0, 11.0). [NP] = 20 mg/L; [PS] = 5 mM; [nZVI/BC_3] = 0.4 g/L. Triangles represent the DMPO-$SO_4^{\cdot-}$ and Circles represent the DMPO-·OH.

for NP degradation at pH 3.0. At initial pH 7.0, NP degradation efficiency decreased to 15.54% and 39.61% by adding EtOH and TBA, respectively, demonstrating that both $SO_4^{\cdot-}$ and ·OH were confirmed to be the predominant reactive species responsible for NP degradation in nZVI/BC_3-PS system. As depicted in Table 2, the radical quenching effect of TBA was higher at pH 11.0, showing that more ·OH radicals were generated, which were responsible for the degradation of NP in nZVI/BC_3-PS system.

A classic radical trapping agent, 5,5-dimethylpyrroline-N-oxide (DMPO) was employed to capture the radical species. Fig. 7 showed the hyperfine splitting constants of free radicals DMPO adduct in nZVI/BC-PS system. The signals of DMPO-$SO_4^{\cdot-}$ and DMPO-HO· adducts with hyperfine splitting constants were a_N = 13.8 G and a_H = 9.8 G, a_H = 1.44 G and a_H = 0.76 and a_N = 15.0 G and a_H = 14.8 G, respectively. The generation of $SO_4^{\cdot-}$ adducts with hyperfine splitting and ·OH can be recognized by hyperfine splitting peaks of DMPO-$SO_4^{\cdot-}$ and DMPO-·OH, respectively [23,52]. The results showed that $SO_4^{\cdot-}$ was a predominant radical at pH 3.0 and 7.0 and played a significant role in the degradation of NP. When pH of nZVI/BC_3-PS system increased to pH 11.0, DMPO-·OH adducts with four split lines appeared which obviously revealing ·OH production at pH 11.0. The results revealed that more ·OH produced with increasing solution pH which favored the production of ·OH.

3.7. Mechanistic study

In order to observe the persulfate activation mechanism in nZVI/BC system, the concentration of dissolved iron (Fe^{2+} and Fe^{3+}) were measured under optimal condition with initial 0.4 g/L nZVI/BC_3, and 5.0 mM PS. As depicted in Fig. 8a, the concentration of Fe^{2+} was rapidly increased in the beginning and then started to decrease progressively to relatively stable. This observation showed the decomposition efficiency of PS. It can be seen that the concentrations of Fe^{2+} and Fe^{3+} were 9.9 mg/L and 20.1 mg/L, respectively after 120 min. The results revealed that the nZVI transformed into dissolved iron (Fe^{2+} and Fe^{3+}) in the presence of PS and most of the iron was Fe^{3+} because nZVI highly corroded by PS. However, 9.4 mg/L nZVI was transferred into dissolved iron in the absence of PS. As mentioned above, 61.7% NP degradation efficiency was observed in nZVI/PS system, which is higher as compared to nZVI alone by adsorption after 120 min. The results demonstrated that PS could be activated indirectly by firstly releasing Fe^{2+} from nZVI into the aqueous systems (Eqs. (2)–(4)), and then the released Fe^{2+} activate persulfate directly to produce free radicals. nZVI can be able to directly activate PS to generate

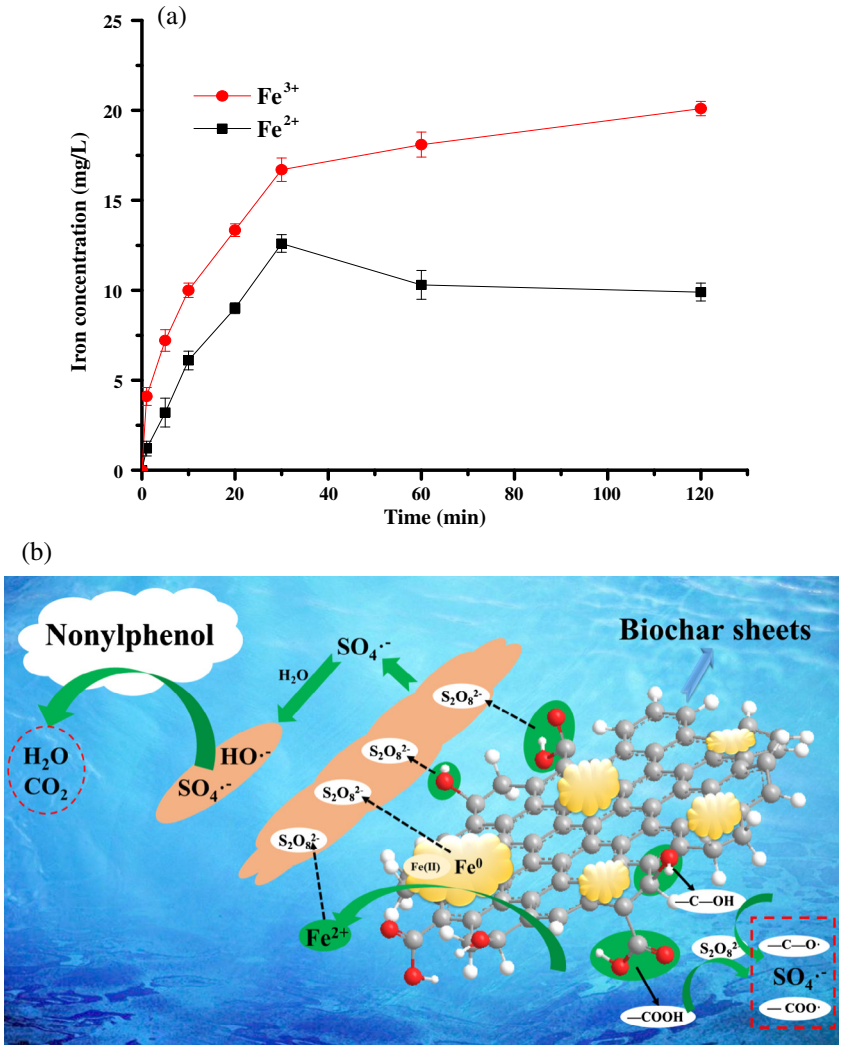

Fig. 8. **(a)** Concentration of Fe^{2+} and Fe^{3+} in nZVI/BC_3-PS system [NP] = 20 mg/L; [PS] = 5.0 mM; Temp. = 25 °C; [nZVI/BC_3] = 0.4 g/L pH = 7.0. **(b)** Proposed mechanism of NP degradation by nZVI/BC nanocomposite activation of persulfate.

$SO_4^{\cdot-}$ and ·OH through electron transfer because nZVI itself works as the electron donor as well (Eqs. (18) and (19)).

$$Fe^0 + 2S_2O_8^{2-} \rightarrow Fe^{2+} + 2SO_4^{\cdot-} + 2SO_4^{2-} \quad (18)$$

$$Fe^0 + S_2O_8^{2-} + 2H_2O \rightarrow 2SO_4^{2-} + Fe^{2+} + 2{\cdot}OH + 2H^+ \quad (19)$$

Al-Shamsi and Thomson [10] observed that iron sulfate might be formed and induced PS decomposition to produce $SO_4^{\cdot-}$ in nZVI /PS system. Two mechanisms proposed for the formation by $FeSO_4$. In first method, $FeSO_4$ could form by the direct reaction of nZVI with SO_4^{2-} (Eq. (20)). In other process, Fe^{2+} in aqueous system converted to Fe^{3+} under anaerobic conditions. $Fe(OH)_3$ formed as an intermediate product by the adsorption of Fe^{3+} on nZVI surface, and then formed FeOOH. $FeSO_4$ was formed by the reaction of FeOOH and SO_4^{2-}. The above processes can be seen in the following reactions [10,53].

$$Fe^0_{(s)} + SO_4^{2-} + 2H_2O \rightarrow FeSO_{4(s)} + 2OH^- + H_{2(g)} \quad (20)$$

$$Fe^{2+} + H_2O \rightarrow Fe^{3+} + OH^- + \frac{1}{2}H_2 \quad (21)$$

$$Fe^{3+} + 3OH^- \rightarrow Fe(OH)_3 \quad (22)$$

$$Fe^{3+} + 3H_2O \rightarrow Fe(OH)_3 + 3H^+ \quad (23)$$

$$Fe(OH)_3 \rightarrow FeOOH + H_2O \quad (24)$$

$$FeOOH + SO_4^{2-} + H_2O \rightarrow FeSO_{4(s)} + 2OH^- + H_2 + O_2 \quad (25)$$

The degradation efficiency of NP was 28.3% in BC-PS system which was higher than NP removal (10.9%) with BC alone system by adsorption. It showed that BC surface had the capacity to activate PS to generate $SO_4^{\cdot-}$ in the absence of nZVI (Eqs. (26) and (27)) because BC surface contains oxygen functional groups (BC-COOH or BC-OH) [38,54].

$$BC\text{-}OOH + S_2O_8^{2-} \rightarrow BC\text{-}OO^{\cdot} + SO_4^{\cdot-} + HSO_4^- \quad (26)$$

$$BC\text{-}OH + S_2O_8^{2-} \rightarrow BC - O^{\cdot} + SO_4^{\cdot-} + HSO_4^- \quad (27)$$

Based on the above results, we propose the mechanism of PS activation in the presence of nZVI/BC nanocomposite (Fig. 8b). Firstly, nZVI well dispersed on BC surface without agglomeration, and the conversion of nZVI to Fe^{2+} accelerated in solution, thus promoting decomposition of PS to produce $SO_4^{\cdot-}$. The generation of $SO_4^{\cdot-}$ from PS was also occurred by the exposed activation sites of Fe^{2+} on nZVI/BC surface. The regeneration of Fe^{2+} carried out

through Fe^{3+} reaction with nZVI surface or in the pores of nZVI/BC composite. Furthermore, the presence of C-OOH and C-OH groups on BC surface would release organic radicals to generate $SO_4^{\cdot-}$. The role of BC in nZVI/BC-PS system is important because the effect of BC is significant, not only for the direct decomposition of persulfate, but also for the acceleration of persulfate mediated by nZVI. It is suggested that the use of nZVI/BC_3 nanocomposite is very effective to enhance the generation of $SO_4^{\cdot-}$ in nZVI/BC_3-PS system, which results higher catalytic ability of nZVI/BC_3. Furthermore, BC has oxygen functional groups, large surface area, abundance pores, which can provide active sites for the activation of PS promoting the degradation of NP by $SO_4^{\cdot-}$ efficiently. Generally, efficient degradation of NP was achieved by nZVI/BC_3-PS system due to synergetic effect of nZVI and BC.

3.8. Stability of nZVI/BC

The stability and reusability of the catalyst is an important factor which needs to be assessed. The stability experiments were conducted for five successive cycles under the following conditions of 2 mg/L NP, 0.4 g/L nZVI/BC_3, 5 mM PS for a reaction period of 120 min. After every run, the catalyst was filtered and washed with deionized water (3 times) and then washed with ethanol before being dried. The degradation efficiencies of NP for every recycle steadily decreased. It can be seen in Fig. 9, the removal efficiency of NP decreased from 96.2% to 74.54% after 5 cycles. The results showed that NP degradation efficiency was still over 74.54% after fifth cycle in nZVI/BC_3-PS system. The decrease in nZVI/BC_3 efficiency can be attributed to following reasons: (1) adsorption of NP on the surface of nZVI/BC_3 which prevented the contact of the catalyst and persulfate; (2) Fe^{2+} leaching will result in the decrease of active sites on the nZVI/BC_3 surface. It shows that the nZVI/BC is a promising catalyst of high stability.

3.9. NP mineralization

The goal of the degradation of any pollutant is not only the pollutant degradation but also to obtain mineralization. In this perspective, NP mineralization was analyzed by measuring the TOC concentration from samples taken at regular time intervals. Fig. 10 showed NP degradation efficiency and mineralization as a function of time at initial NP concentration 20 mg/L, PS concentration 5 mM, pH 7.0, nZVI/BC_3 dosage 0.4 g/ L and a temperature of 25 °C. As can be seen in Fig. 3b, the degradation efficiency of NP reached 78% after 30 min while the mineralization of NP was 31%

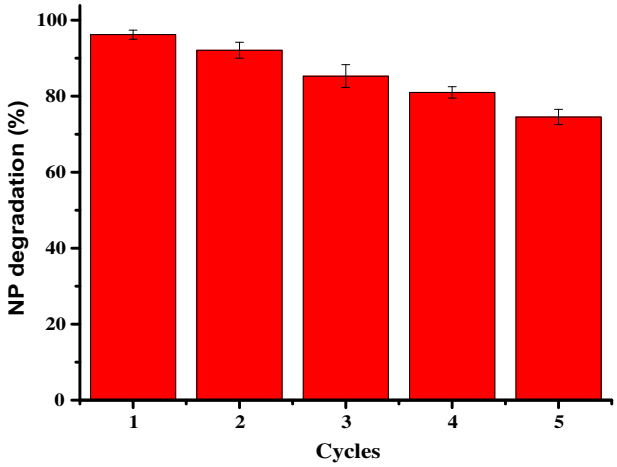

Fig. 9. Reusability study of nZVI/BC_3 nanocomposite for NP degradation [NP] = 20 mg/L; [PS] = 5.0 mM; Temp. = 25 °C; [nZVI/BC_3] = 0.4 g/L; pH = 7.0.

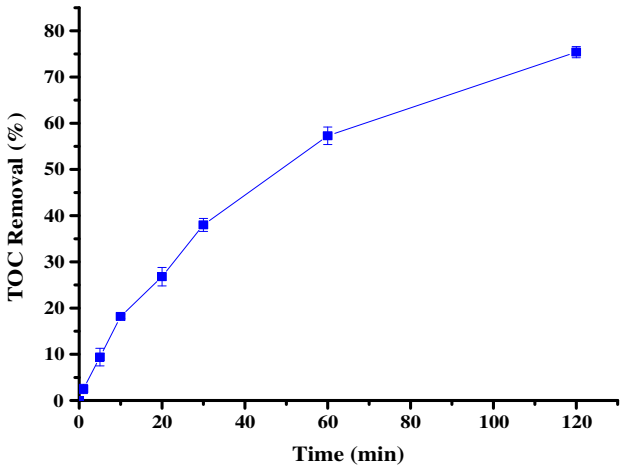

Fig. 10. TOC removal [NP] = 20 mg/L; [PS] = 5.0 mM; Temp. = 25 °C; [nZVI/BC_3] = 0.4 g/L pH = 7.0.

at that time. However, the mineralization of NP enhanced with passage of time and 73.4% NP was mineralized after 120 min. It showed that compared to degradation efficiency, a longer time is required to attain higher mineralization efficiency.

4. Conclusions

This study reveals the successful synthesis and characterization of nZVI/BC nanocomposite. nZVI/BC nanocomposite was synthesized using low-cost abundant rice husk through reduction of ferrous iron with sodium borohydride as a reductant under nitrogen atmosphere. The nanocomposite was utilized as a promising activator of persulfate for the degradationof NP in aqueous solution. The results revealed that nZVI/BC_3 appeared to provide the best performance with the NP degradation efficiency of 96.2%. The degradation efficiency of NP was significantly influenced by nZVI/BC_3 dosage, initial pH and PS concentration. The generation of $SO_4^{\cdot-}$ promoted by redox effect of Fe^{2+}/Fe^{3+} and transfer of electron from oxygen functional groups present on the surface of BC. EPR results demonstrated that both $SO_4^{\cdot-}$ and $^{\cdot}OH$ were responsible for the degradation of NP. This study provides a promising approach towards the use of nZVI/BC as an efficient activator of PS for the treatment of wastewater containing various organic contaminants.

Acknowledgements

This work was financially supported by the National Natural Science Foundation of China (51572089), the National Natural Science Foundation of Guangdong Province, China (2015A030313232), the Foundation of Science and Technology Planning Project of Guangdong Province (2016A050502007) the Research Funds of State Key Lab of Subtropical Building Science, South China University of Technology (2015ZB25) and the Funds of the State Key Laboratory of Pulp and Paper Engineering, China (201477).

References

[1] A. Soares, B. Guieysse, B. Jefferson, E. Cartmell, J.N. Lester, Nonylphenol in the environment: a critical review on occurrence, fate, toxicity and treatment in wastewaters, Environ. Int. 34 (2008) 1033–1049.
[2] J. Shan, B. Jiang, B. Yu, C. Li, Y. Sun, H. Guo, J. Wu, E. Klumpp, A. Schäffer, R. Ji, Isomer-specific degradation of branched and linear 4-nonylphenol isomers in an oxic soil, Environ. Sci. Technol. 45 (2011) 8283–8289.
[3] O. Bechambi, W. Najjar, S. Sayadi, The nonylphenol degradation under UV irradiation in the presence of Ag–ZnO nanorods: effect of parameters and degradation pathway, J. Taiwan Inst. Chem. Eng. 60 (2016) 496–501.

[4] J. Peng, G. Wang, D. Zhang, D. Zhang, X. Li, Photodegradation of nonylphenol in aqueous solution by simulated solar UV-irradiation: the comprehensive effect of nitrate, ferric ion and bicarbonate, J. Photochem. Photobiol., A 326 (2016) 9–15.
[5] L.J. Xu, W. Chu, P.-H. Lee, J. Wang, The mechanism study of efficient degradation of hydrophobic nonylphenol in solution by a chemical-free technology of sonophotolysis, J. Hazard. Mater. 308 (2016) 386–393.
[6] G. Bertanza, R. Pedrazzani, M. Dal Grande, M. Papa, V. Zambarda, C. Montani, N. Steimberg, G. Mazzoleni, D. Di Lorenzo, Effect of biological and chemical oxidation on the removal of estrogenic compounds (NP and BPA) from wastewater: an integrated assessment procedure, Water Res. 45 (2011) 2473–2484.
[7] M. Zhang, X. Chen, H. Zhou, M. Murugananthan, Y. Zhang, Degradation of p-nitrophenol by heat and metal ions co-activated persulfate, Chem. Eng. J. 264 (2015) 39–47.
[8] S.-Y. Oh, S.-G. Kang, P.C. Chiu, Degradation of 2,4-dinitrotoluene by persulfate activated with zero-valent iron, Sci. Total Environ. 408 (2010) 3464–3468.
[9] I. Hussain, Y. Zhang, S. Huang, X. Du, Degradation of p-chloroaniline by persulfate activated with zero-valent iron, Chem. Eng. J. 203 (2012) 269–276.
[10] A.M. Al-Shamsi, N.R. Thomson, Treatment of organic compounds by activated persulfate using nanoscale zero valent iron, Ind. Eng. Chem. Res. 52 (2013) 13564–13571.
[11] C. Cai, Z. Zhang, H. Zhang, Electro-assisted heterogeneous activation of persulfate by Fe/SBA-15 for the degradation of Orange II, J. Hazard. Mater. 313 (2016) 209–218.
[12] D.H. Han, J.Q. Wan, Y.W. Ma, Y. Wang, Y. Li, D. Li, Z.Y. Guan, New insights into the role of organic chelating agents in Fe(II) activated persulfate processes, Chem. Eng. J. 269 (2015) 425–433.
[13] I. Hussain, Y. Zhang, S. Huang, Q. Gao, Degradation of p-chloroaniline by FeO3-xH3-2x/Fe0 in the presence of persulfate in aqueous solution, in: RSC Adv. 5 (2015) 41079–41087.
[14] A. Ghauch, A. Tuqan, Oxidation of bisoprolol in heated persulfate/H2O systems: kinetics and products, Chem. Eng. J. 183 (2012) 162–171.
[15] C. Tan, N. Gao, Y. Deng, W. Rong, S. Zhou, N. Lu, Degradation of antipyrine by heat activated persulfate, Sep. Purif. Technol. 109 (2013) 122–128.
[16] X. Xie, Y. Zhang, W. Huang, S. Huang, Degradation kinetics and mechanism of aniline by heat-assisted persulfate oxidation, J. Environ. Sci. 24 (5) (2012) 821–826.
[17] W.H. Chu, D.M. Li, N.Y. Gao, M.R. Templeton, C.Q. Tan, Y.Q. Gao, The control of emerging haloacetamide DBP precursors with UV/persulfate treatment, Water Res. 72 (2015) 340–348.
[18] S. Rodriguez, L. Vasquez, D. Costa, A. Romero, A. Santos, Oxidation of Orange G by persulfate activated by Fe(II), Fe(III) and zero valent iron, ZVI, Chemosphere 101 (2014) 86–92.
[19] Y.F. Rao, L. Qu, H.S. Yang, W. Chu, Degradation of carbamazepine by Fe(II)-activated persulfate process, J. Hazard. Mater. 268 (2014) 23–32.
[20] L. Bingzhi, L. Lin, L. Kuangfei, Z. Wei, L. Shuguang, L. Qishi, Removal of 1,1,1-trichloroethane from aqueous solution by a sono-activated persulfate process, Ultrason. Sonochem. 20 (2013) 855–863.
[21] O.S. Furman, A.L. Teel, R.J. Watts, Mechanism of base activation of persulfate, Environ. Sci. Technol. 44 (2010) 6423–6428.
[22] A. Tsitonaki, B. Petri, M. Crimi, H. Mosbaek, R.L. Siegrist, P.L. Bjerg, In situ chemical oxidation of contaminated soil and groundwater using persulfate: a review, Crit. Rev. Environ. Sci. Technol. 40 (2010) 55–91.
[23] G.D. Fang, J. Gao, D.D. Dionysiou, C. Liu, D.M. Zhou, Activation of persulfate by quinones: free radical reactions and implication for the degradation of PCBs, Environ. Sci. Technol. 47 (2013) 4605–4611.
[24] J. Zhao, Y. Zhang, X. Quan, S. Chen, Enhanced oxidation of 4-chlorophenol using sulfate radicals generated from zero-valent iron and peroxydisulfate at ambient temperature, Sep. Purif. Technol. 71 (2010) 302–307.
[25] S.-Y. Oh, H.W. Kim, J.-M. Park, H.-S. Park, C. Yoon, Oxidation of polyvinyl alcohol by persulfate activated with heat, Fe^{2+}, and zero-valent iron, J. Hazard. Mater. 168 (2009) 346–351.
[26] I. Hussain, Y. Zhang, S. Huang, Degradation of aniline with zero-valent iron as an activator of persulfate in aqueous solution, RSC Adv. 4 (2014) 3502–3511.
[27] Q. Wang, Y. Shao, N. Gao, W. Chu, J. Deng, X. Shen, X. Lu, Y. Zhu, X. Wei, Degradation of alachlor with zero-valent iron activating persulfate oxidation, J. Taiwan Inst. Chem. Eng. 63 (2016) 1–7.
[28] J. Zhan, T. Zheng, G. Piringer, C. Day, G.L. McPherson, Y. Lu, K. Papadopoulos, V. T. John, Transport characteristics of nanoscale functional zerovalent iron/silica composites for in situ remediation of trichloroethylene, Environ. Sci. Technol. 42 (2008) 8871–8876.
[29] S. Luo, P.F. Qin, J.H. Shao, L. Peng, Q.R. Zeng, J.D. Gu, Synthesis of reactive nanoscale zero valent iron using rectorate supports and its application for Orange II removal, Chem. Eng. J. 223 (2013) 1–7.
[30] H. Park, Y.M. Park, K.M. Yoo, S.H. Lee, Reduction of nitrate by resin supported nanoscale zero-valent iron, Water Sci. Technol. 59 (2009) 2153–2157.
[31] K. Mackenzie, S. Bleyl, A. Georgi, F.D. Kopinke, Carbo-Iron-An Fe/AC composite—as alternative to nano-iron for groundwater treatment, Water Res. 46 (2012) 3817–3826.
[32] S. Fukuchi, R. Nishimoto, M. Fukushima, Q.Q. Zhu, Effects of reducing agents on the degradation of 2,4,6-tribromophenol in a heterogeneous Fenton-like system with an iron-loaded natural zeolite, Appl. Catal. B Environ. 147 (2014) 411–419.
[33] S. Kumar, A.K. Singh, A.K. Dasmahapatra, T.K. Mandal, D. Bandyopadhyay, Graphene based multifunctional superbots, Carbon 89 (2015) 31–40.
[34] D. Mohan, A. Sarswat, Y.S. Ok, C.U. Pittman-Jr, Organic and inorganic contaminants removal from water with biochar, a renewable, low cost and sustainable adsorbent – a critical review, Bioresour. Technol. 160 (2014) 191–201.
[35] M. Ahmad, A.U. Rajapaksha, J.E. Lim, M. Zhang, N. Bolan, D. Mohan, M. Vithanage, S.S. Lee, Y.S. Ok, Biochar as a sorbent for contaminant management in soil and water: a review, Chemosphere 99 (2014) 19–33.
[36] Y. Yao, B. Gao, J.J. Chen, M. Zhang, M. Inyang, Y.C. Li, A. Alva, L.Y. Yang, Engineered carbon (biochar) prepared by direct pyrolysis of mg-accumulated tomato tissues: characterization and phosphate removal potential, Bioresour. Technol. 138 (2013) 8–13.
[37] Y.M. Zhou, B. Gao, A.R. Zimmerman, H. Chen, M. Zhang, X.D. Cao, Biochar supported zero valent iron for removal of various contaminants from aqueous solutions, Bioresour. Technol. 152 (2014) 538–542.
[38] J. Yan, L. Han, W. Gao, S. Xue, M. Chen, Biochar supported nanoscale zerovalent iron composite used as persulfate activator for removing trichloroethylene, Bioresour. Technol. 175 (2015) 269–274.
[39] APHA, AWWA and WEF, Standards Methods for the Examination of Water and Wastewater, Washington, DC, 1998.
[40] C.J. Liang, C.F. Huang, N. Mohanty, R.M. Kurakalva, A rapid spectrophotometric determination of persulfate anion in ISCO, Chemosphere 73 (2008) 1540–1543.
[41] H.C. Gao, F. Xiao, C.B. Ching, H.W. Duan, One-Step electrochemical synthesis of PtNi nanoparticle-graphene nanocomposites for nonenzymatic amperometric glucose detection, ACS Appl. Mater. Interfaces 3 (2011) 3049–3057.
[42] Z.G. Liu, F.S. Zhang, J.Z. Wu, Characterization and application of chars produced from pinewood pyrolysis and hydrothermal treatment, Fuel 89 (2010) 510–514.
[43] P. Devi, A.K. Saroha, Synthesis of the magnetic biochar composites for use as an adsorbent for the removal of pentachlorophenol from the effluent, Bioresour. Technol. 169 (2014) 525–531.
[44] J. Xu, N. Gao, Y. Tang, Y. Deng, M. Sui, Perchlorate removal using granular activated carbon supported iron compounds: synthesis, characterization and reactivity, J. Environ. Sci. 22 (2010) 1807–1813.
[45] J.J. Chen, J.X. Zhu, Z.L. Da, H. Xu, J. Yan, H.Y. Jia, H.M. Shu, H.M. Li, Improving the photocatalytic activity and stability of graphene-like BN/AgBr composites, Appl. Surf. Sci. 313 (2014) 1–9.
[46] M.C. Hua, K.S. Hui, K.N. Hui, Role of graphene in MnO_2/graphene composite for catalytic ozonation of gaseous toluene, Chem. Eng. J. 254 (2014) 237–244.
[47] C. Cai, L.G. Wang, H. Gao, L.W. Hou, H. Zhang, Ultrasound enhanced heterogeneous activation of peroxy disulfate by bimetallic Fe–Co/GAC catalyst for the degradation of acid orange 7 in water, J. Environ. Sci. 26 (2014) 1267–1273.
[48] B. Lai, Z. Chen, Y. Zhou, P. Yang, J. Wang, Z. Chen, Removal of high concentration p-nitrophenol in aqueous solution by zero valent iron with ultrasonic irradiation (US–ZVI), J. Hazard. Mater. 250–251 (2013) 220–228.
[49] A. Ghauch, A.M. Tuqan, N. Kibbi, Naproxen abatement by thermally activated persulfate in aqueous systems, Chem. Eng. J. 279 (2015) 861–873.
[50] G.P. Anipsitakis, D.D. Dionysiou, Radical generation by the interaction of transition metals with common oxidants, Environ. Sci. Technol. 38 (2004) 3705–3712.
[51] P. Xie, J. Ma, W. Liu, J. Zou, S. Yue, X. Li, M.R. Wiesner, J. Fang, Removal of 2-MIB and geosmin using UV/persulfate: contributions of hydroxyl and sulfate radicals, Water Res. 69 (2015) 223–233.
[52] X.G. Duan, H.Q. Sun, J. Kang, Y.X. Wang, S. Indrawirawan, S.B. Wang, Insights into heterogeneous catalysis of persulfate activation on dimensional structured nanocarbons, ACS Catal. 5 (2015) 4629–4636.
[53] X.Q. Li, J. Cao, W.X. Zhang, Stoichiometry of Cr(VI) immobilization using nanoscale zero valent iron (nZVI): a study with high-resolution X-ray photoelectron spectroscopy (HR-XPS), Ind. Eng. Chem. Res. 47 (2008) 2131–2139.
[54] L. Zhou, J. Ma, H. Zhang, Y. Shao, Y. Li, Fabrication of magnetic carbon composites from peanut shells and its application as a heterogeneous Fenton catalyst in removal of methylene blue, Appl. Surf. Sci. 324 (2015) 490–498.